



**HAL**  
open science

## Computational Modelling of Metastasis Development in Renal Cell Carcinoma

Etienne Baratchart, Sébastien Benzekry, Andreas Bikfalvi, Thierry Colin, Lindsay S. Cooley, Raphaël Pineau, Emeline J Ribot, Olivier Saut, Wilfried Souleyreau

► **To cite this version:**

Etienne Baratchart, Sébastien Benzekry, Andreas Bikfalvi, Thierry Colin, Lindsay S. Cooley, et al.. Computational Modelling of Metastasis Development in Renal Cell Carcinoma. PLoS Computational Biology, 2015, 11 (11), 10.1371/journal.pcbi.1004626 . hal-01164834v1

**HAL Id: hal-01164834**

**<https://inria.hal.science/hal-01164834v1>**

Submitted on 17 Jun 2015 (v1), last revised 25 Nov 2015 (v2)

**HAL** is a multi-disciplinary open access archive for the deposit and dissemination of scientific research documents, whether they are published or not. The documents may come from teaching and research institutions in France or abroad, or from public or private research centers.

L'archive ouverte pluridisciplinaire **HAL**, est destinée au dépôt et à la diffusion de documents scientifiques de niveau recherche, publiés ou non, émanant des établissements d'enseignement et de recherche français ou étrangers, des laboratoires publics ou privés.

# Computational modelling of metastasis development in renal cell carcinoma

Etienne Baratchart<sup>1</sup>, Sébastien Benzekry<sup>1,\*</sup>, Andreas Bikfalvi<sup>2,\*</sup>, Thierry Colin<sup>1,\*</sup>, Lindsay S. Cooley<sup>2</sup>, Raphaël Pineau<sup>2</sup>, Emeline Ribot<sup>3</sup>, Olivier Saut<sup>1</sup>, Wilfried Souleyreau<sup>2</sup>

<sup>1</sup> INRIA Equipe Projet MONC, Institut mathématique de Bordeaux UMR 5251, Université de Bordeaux, Talence

<sup>2</sup> LAMC University Bordeaux, INSERM U1029 University Bordeaux, Pessac

<sup>3</sup> Centre de Résonance Magnétique des Systèmes Biologiques, UMR 5536, CNRS/Université de Bordeaux Segalen, Bordeaux

**Authors are listed in alphabetical order**

**\* Corresponding authors**

**E-mail:** [sebastien.benzekry@inria.fr](mailto:sebastien.benzekry@inria.fr), [Thierry.Colin@math.u-bordeaux1.fr](mailto:Thierry.Colin@math.u-bordeaux1.fr), [andreas.bikfalvi@u-bordeaux.fr](mailto:andreas.bikfalvi@u-bordeaux.fr)

## **Abstract**

To improve our understanding of the biology of the metastatic colonization process, we conducted a modelling study based on multi-modal data from an orthotopic murine experimental system of metastatic renal cell carcinoma. The standard theory of metastatic colonization usually assumes that secondary tumours, once established at a distant site, grow independently from each other and from the primary tumour. Using a mathematical model describing the metastatic population dynamics under this assumption, we challenged the theory against our data that included: 1) dynamics of primary tumour cells in the kidney and metastatic cells in the lungs, retrieved by green fluorescent protein tracking, and 2) magnetic resonance images (MRI) informing on the number and size of macroscopic lesions. While the model could fit the primary tumour and total metastatic burden, the predicted size distribution was not in agreement with the MRI observations. Moreover, the model was incompatible with the growth rates of individual metastatic tumours.

To explain the observed metastatic patterns, we hypothesised that metastatic foci derived from one or a few cells could aggregate, resulting in a similar total mass but a smaller number of metastases. This was indeed observed in our data and led us to investigate the effect of spatial interactions on the dynamics of the global metastatic burden. We derived a novel mathematical model for spatial tumour growth, where the intra-tumour increase in pressure is responsible for the slowdown of the growth rate. The model could fit the growth of lung metastasis visualized by magnetic resonance imaging. As a non-trivial outcome from this analysis, the model predicted that the net growth of two neighbouring tumour lesions that enter in contact is considerably impaired (of  $31\% \pm 1.5\%$ , mean  $\pm$  standard deviation), as compared to the growth of two independent tumours. Together, our results have implications for theories of metastatic development and suggest that global dynamics of metastasis development is dependent on spatial interactions between metastatic lesions.

## **Author Summary**

We used mathematical modelling to formalize the standard theory of metastatic initiation, under which secondary tumours, after establishment in a distant organ, grow independently from each other and from the primary tumour. When calibrated on the experimental data of primary tumour and total metastatic burden in the lungs in an animal model of renal cell carcinoma, the initial model predicted a size distribution of metastatic foci that did not fit with observations obtained experimentally using magnetic resonance imaging (which provided size and number of macro-metastases). The model predicted an increase in the number of lesions, but of smaller size when compared to the data. Two hypotheses may explain our findings: 1) small metastatic foci merge into larger ones and/or 2) circulating tumour cells may join already established tumours. This led us to revise the standard theory and to derive a spatial model of tumour growth in order to explore the quantitative implications of tumours merging on global tumour growth.

## Introduction

Metastasis, the spread of a primary tumour to secondary location(s) in the body, is the ultimate cause of death for the majority of cancer patients. Although studied for more than 180 years [1], increasing efforts in recent years contributed to a better understanding of this aspect of tumour development [2,3], with exciting new discoveries [4–7] that potentially have important clinical implications. The metastatic process can be coarsely divided into two major phases: 1) dissemination of detaching cells from the primary tumour to a secondary site and 2) colonization of this distant organ [8,9]. While the former has been relatively well elucidated (in particular due to recent advances about the epithelial-to-mesenchymal transition) [10], the latter remains not fully understood, especially during the initiation phase [9]. This is due, in part, to experimental limitations that hinder our ability to observe colonization of organs by tumour cells and the development of tumour lesions.

In this context, mathematical models provide powerful tools to potentiate data analysis, infer hidden information, test biological hypotheses against the empirical data and simulate a range of conditions that may be confronted to the biological reality. In recent years, several spatial models for tumour growth have been developed [11,12] and parameter estimation techniques were introduced to confront the models to imaging data [13]. However, despite a large body of literature for modelling tumour growth [14,15], relatively little effort has been devoted to the development and validation of mathematical models describing the biology of the metastatic process (see [16,17] for an early and notable exception and [18] for a recent review). Iwata and colleagues have proposed a simple mathematical model for the growth of a population of metastatic colonies [19], which was recently shown able to fit experimental data describing the increase in total metastatic burden [20,21]. In this mathematical description, each metastasis grows independently from the others and from the primary tumour. However, in a space-limited organ (such as the lungs), where two neighbouring metastatic foci are growing in close vicinity, they might enter in contact and interactions occur, ultimately leading to the merging of the metastatic foci. This phenomenon is not taken into account in a classical description of metastasis development, although this can lead to important differences in the number and sizes of the colonies.

We report herein a theoretical study to test this hypothesis using *in vivo* data derived from a metastatic renal carcinoma model in mice. We first show that the naive theory of metastatic initiation in which distinct foci grow independently from each other (as assumed in [19,20]) predicts an unrealistically large number of metastases. We conducted, next, a quantitative study taking into account the interactions between two neighbouring tumours using a spatial model of tumour growth. This model, based on a pressure-mediated growth law, was fitted to magnetic resonance imaging data of metastatic tumour growth. Simulations of the effect of the mechanical interactions on global tumour growth revealed significant impact of these interactions on the global growth and allowed to test if merging by passive motion could explain the data that are not in accordance with the classical model.

## Results

### Modelling approach integrating experimental data

We first calibrated a mathematical model of tumour growth and metastatic dissemination using quantitative data derived from Green fluorescent protein (GFP)-tracking of primary and metastatic tumours (see Materials and methods). In a second step, we estimated the number and the sizes of metastatic lesions and compared them to those observed by Magnetic Resonance Imaging (MRI).

***Growth rates of individual metastatic tumours:*** RENCA cells were injected orthotopically sub-capsularly in the kidney. The first metastatic cells were observed in the lungs at day 14 and the first macro-metastases at day 18 (Fig 1). No metastasis was observed in other organs.

#### **Fig 1. The animal model**

At day 14 after GFP+ RENCA cells injection, the first tumour cells were observed in the lungs; At day 18, the first macro-metastases were observed at MRI.

Assuming in a theoretical model that each metastasis originates from one surviving cell would imply that some metastases grow from the volume of one cell ( $\approx 10^{-6}$  mm<sup>3</sup>, according to the well-established conversion rule 1 mm<sup>3</sup>  $\approx$  10<sup>6</sup> cells [22]), to a volume of few mm<sup>3</sup> (between 0.02 and 2.5 mm<sup>3</sup>) in five days at most. This would give a cell doubling time comprised between 5.7 and 8.3 hours, which represents less than one third of the doubling time that is observed *in vitro* that lasts 24.5 hours [23]. This doubling time would also have to remain constant during 5 days. Such a fast growth is highly improbable. Moreover, the doubling time is increasing during *in vivo* growth [15], which would imply even shorter doubling times in order to fit the data. Therefore, the naive theory consisting in describing each metastasis with a tumour expansion process only based on cell proliferation seems unlikely. One could argue that metastatic foci could arise from cell clumps rather than a single cell. However, the same calculation starting with an initial number of cells as high as 500 still leads to an unlikely short doubling time (of 10 hours).

***Primary kidney tumour and the dynamics of lung metastasis:*** The standard theory of metastatic development assumes that secondary tumours are seeded from the primary tumour and that, once established at the distant sites (the lungs in our case), they grow independently from each other and from the rest of the organism [1,2,10,24–26]. We tested this theory against the following data: a) dynamics of the increase of GFP+ tumour cells in the kidney, b) longitudinal quantification of GFP+ tumour cells in the lungs and c) MRI images of lung metastasis. To this aim, we formalized the standard theory into a mathematical model. The model was then fitted to the data a) and b) and predictions were compared to the data c).

*Mathematical modelling:*

The standard theory as described above has been mathematically formalized by Iwata et al. [19]. This model was reported to provide a valid description of the dynamics of total metastatic burden in two animal models, including ours (human breast carcinoma xenograft [20,21] and syngeneic renal cell carcinoma [21]).

The model was adapted here as follows. We assumed that the GFP signal was proportional to the number of cancer cells, itself proportional to the tumour volume observed by MRI. The primary tumour volume at time  $t$  was denoted  $V_p(t)$  and its growth rate  $g(V_p(t))$ . The primary tumour disseminates metastatic cells into the lungs according to a volume-dependent dissemination law  $d(V_p(t))$ . The metastatic colonies then grow into the lungs according to the same growth law as the primary tumour. The model describes the size distribution of the metastatic lesions at the distant site by means of a size-dependent density  $\rho(t, v)$  of metastatic colonies of size  $v$  at time  $t$ , i.e.  $\rho(t, v)dv$  is the number of metastatic colonies with a size comprised between  $v$  and  $v + dv$ . Secondary emission of metastases (i.e., metastases from metastases) was neglected in our case.

Tumour growth was modelled by means of the Gomp-Exp model [27], which is characterized by two phases: first an exponential phase (with a growth rate given by the *in vitro* proliferation rate), then a Gompertz phase (i.e., exponentially decreasing growth rate). For the primary tumour growth, the model writes

$$\begin{cases} \frac{dV_p}{dt}(t) = g(V_p(t)) \\ V_p(0) = V_{inj} \\ g(V_p) = \min(\lambda V_p, (\alpha - \beta \ln(V_p)) V_p) \end{cases} \quad (1)$$

where  $\lambda$  is the *in vitro* proliferation rate of RENCA cells (retrieved from [23]),  $\alpha$  corresponds to the specific growth rate at the size of one unit,  $\beta$  is the rate of exponential decrease of the specific growth rate and  $V_{inj}$  is the amount of injected cells. The Gompertz model has been proven able to describe *in vivo* tumour growth in numerous animal experimental systems [15,28,29], as well as for human data [30]. Adjunction of the initial exponential phase was considered here because the Gompertz model exhibits an infinite relative growth rate for arbitrary small cell numbers, a feature that was not considered relevant, especially for the metastases that start from one cell. At this point we needed to retrieve the GFP signal associated to one cell. To achieve this, we performed a preliminary fit of the primary tumour GFP signals with the parameter  $V_{inj}$  subject to optimization, using population mixed-effects statistical modelling (see Fig S1). We then assumed proportionality between the number of cells injected (100 000) and the estimated signal at day 0. The GFP signal associated to one cell was then derived and is denoted by  $V_0$ . We found  $V_0 = 7.96 \times 10^{-6}$  relative units of GFP signal.

Growth of secondary tumours was assumed to follow the same law (Gomp-Exp) and parameter values. More complex modelling including different growth parameters for the primary tumour and metastasis were tested but did not substantially improve the fits.

At present time, there is no detailed study on the shape that the function  $d$  should have. However, it is often assumed to follow the law [19–21]:

$$d(V_p) = \mu V_p^\gamma$$

where parameter  $\mu$  is related to an intrinsic (genetic) probability of the metastatic potential of the tumour cells, combined to the probability of successfully passing all the steps required for establishment of a metastasis (detachment from the primary tumour, intravasation into the blood circulation, survival in transit, arrest and extravasation at the distant site, establishment of a new colony [2]). Precise identification of the value of parameter  $\gamma$  was not possible on our data set, and in the following analysis, we arbitrarily fixed  $\gamma = 1$ , corresponding to the simplest assumption (emission proportional to the tumour volume). The robustness of the results was assessed with respect to this value by repeating the entire analysis of the data for values of  $\gamma$  ranging from 0 to 1. Similar results were obtained in each case.

Overall, the model writes as a transport equation on  $\rho$ , endowed with suitable boundary and initial conditions [19]:

$$\begin{cases} \partial_t \rho(t, v) + \partial_v (\rho(t, v) g(v)) = 0 & t \in ]0, +\infty[, v \in ]V_0, +\infty[ \\ g(V_0) \rho(t, V_0) = d(V_p(t)) \\ \rho(0, v) = 0 \end{cases}$$

From the solution of this problem, the main quantity of interest for our purpose was the total metastatic burden, defined by

$$M(t) = \int_{V_0}^{+\infty} v \rho(t, v) dv$$

The model output was fitted to the GFP expression data from the lungs (Fig 2).

## Fig 2. The standard theory: primary tumour and metastatic burden dynamics fitting

(A): Fits of the primary tumour and metastatic burden dynamics, under a mathematical model assuming independent growth of each secondary tumour and using mixed-effects modeling for statistical representation of the population distribution of the parameters and measurement error.

(B): Fit on the metastatic burden. PT= Primary Tumour. Met = Metastatic burden. Prct = percentile

### Results:

Due to the large inter-animal variability, we used a nonlinear mixed-effects statistical framework for fitting the model to the data and resulting estimation of the parameters [31] (see also [20,21] for applications to bioluminescence data of metastatic burden), which is particularly well suited for sparse longitudinal data in an animal population. Briefly, this framework considers estimation of a (parametric) distribution of the parameters within the population. This allows pooling all the data points together, thus leading to an increase of the robustness of the estimation

and of the descriptive power for inter-animal variability. For the maximization of likelihood associated to nonlinear mixed-effects modeling, we used a version of a stochastic expectation maximization algorithm implemented in the Matlab function *nlmefitsa* [32]. To simulate the model, a well-adapted method using an integral formulation for  $M(t)$  and the fast Fourier transform algorithm was employed [33]. This ensured reduction of the computational cost of simulations, which was necessary due to the very high number of runs required by *nlmefitsa*.

Data from the primary tumour and the metastatic burden were fitted together, and the model demonstrated satisfactorily descriptive power for the total metastatic burden (Fig 2), in accordance with other studies [20,21]. The calibrated model corresponding to the median population parameters (reported in Table 1) was further used to predict the distribution of macro-metastases visible in the MRI images, and to confront this prediction to the observations. Among the MRI data collected, images of only one mouse were eligible for reliable assessment of the number and sizes of macro-metastases. In this mouse, the smallest detectable metastasis had a volume of  $0.05 \text{ mm}^3$ , which was taken as the minimal visibility threshold, thus defining macro-metastasis as metastasis having a larger size than this value. Results are reported in Fig 3. Critically, the maximal volumes predicted by the model were considerably smaller than those observed by MRI. For example, at  $T = 19$  days, while the total metastatic burden was similar in the data and in the model (Fig 2), the macro-metastatic burden was three-fold larger in the latter than in the former (Fig 3). Additionally, at  $T = 26$  days, the macro-metastatic burden was comparable in the data and in the model, but the standard theory (formalized by the mathematical model) predicted that the largest tumour would have a volume of only  $1.06 \text{ mm}^3$ , while the largest observed metastasis had a volume of  $13.6 \text{ mm}^3$ . On the other hand, the number of metastatic lesions was substantially larger in the model (102 versus 11 in the data). Similar results were also obtained when re-performing the analysis for variable values (between 0 and 1) of parameter  $\gamma$  (results not shown).

**Fig 3. Time course of the macro-metastases size distribution: naive model versus observations**

Top row: Simulation of the mathematical formalism of the naive theory (i.e. dissemination and independent growth of the resulting tumor foci), using the parameter values inferred from the total metastatic burden data (total GFP signal in the lungs). Only tumours larger than the visible threshold at MRI ( $0.05 \text{ mm}^3$ ) were plotted. Bottom row: Observations of macro-metastases numbers and sizes in one mouse on MRI data.

**Table 1: Parameters values resulting from the population fit of the primary tumour and metastatic dynamics.**

Par.	Unit	Median value	95% CI
$\alpha$	$\text{day}^{-1}$	0.417	(0.329 - 0.557)
$\beta$	$\text{day}^{-1}$	0.106	(0.0372 - 0.145)
$\mu$	$\text{cell}^{-1}\text{day}^{-1}$	$9.72 \times 10^{-6}$	$(1.81 - 52.2) \times 10^{-6}$

CI = confidence interval

These results strongly indicate that the standard theory of metastatic progression as described by the model employed here (i.e., dissemination and independent growth), when calibrated to data of total metastatic burden, is in contradiction with the experimental observations with regard to the number of metastatic foci and their size distributions. Two hypotheses could be considered to reconcile the data with the theory: (1) non-trivial interactions between metastases and (2) interactions between the metastatic tumours and the circulating tumour cells (cells attraction). Interestingly, we indeed observed merging of two metastases in our data (between days 21 and 24, see Fig 4) and therefore decided to investigate this further.

#### **Fig 4. Metastases merging**

From left to right: Sagittal slices of the lungs from day 19 until day 26 for the same mouse. Two tumours are growing close to each other and merge between days 21 and 24.

#### **Spatial interactions between metastatic tumours**

We first considered the most basic assumption of an exponential growth law:  $V(t) = V_0 e^{\lambda t}$ . In this case, due to the linearity of the model as a function of  $V_0$ , a tumour starting from size  $2V_0$  has the same size as two independent tumours starting from size  $V_0$ . However, tumour growth exhibits increasing doubling times when increasing in size. If we consider the volume dynamics and model this using the Gompertz law, then, due to the nonlinearity of the model, merging two tumour lesions into one (in summing their volumes) leads to a slower growth and ultimately smaller volume compared to two tumours that are growing separately (Fig S2). Yet, under the Gompertz law, spatial interactions are not taken into account, while they are probably of great importance. This motivated us to study the global impact of spatial interactions and to propose a spatial model of tumour growth.

**Advection-type modelling of growth and movement:** The two-dimensional model we used for the spatial growth describes a saturated flow in a porous medium comprising two entities, the tumour tissue and the healthy tissue, with  $P$  denoting the tumour cell density and  $S$  the healthy cell density. The third variable is a pressure field  $\Pi$ . The model describes, on a domain  $\Omega$ , the passive motion of the tissues due to the increase in volume caused by proliferation. Writing a mass-balance equation, this corresponds to the following:

$$\frac{\partial P}{\partial t}(t, x) + \nabla \cdot (v(t, x)P(t, x)) = \gamma(t, x, P, S, \Pi)P(t, x) \quad (2)$$

$$\frac{\partial S}{\partial t}(t, x) + \nabla \cdot (v(t, x)S(t, x)) = 0 \quad (3)$$

where  $\gamma$  is the growth rate of the proliferating cells. We also assumed that the flow is saturated, with  $P + S = 1$  at each point of the domain. Summing (2) and (3) leads to the following condition on the velocity of the flow:

$$\nabla \cdot v = \gamma P \quad (4)$$

This condition means that the tumour volume changes are due to proliferation. We considered the organ (the lungs) as a porous medium with a porosity  $k(t, x)$  and that the velocity  $v$  is due to pressure gradients within the tumour. Therefore, we modelled the velocity flow by a Darcy law, as Preziosi and Ambrosi in [34]:

$$v = -k\nabla\Pi \quad (5)$$

The velocity  $v$  is the passive motion velocity, due to the pressure exerted by the proliferative tissue on the surrounding tissues. These tissues are in this way "pushed" and move away from the high-pressure areas to the lower-pressure ones.

The size of the computational domain  $\Omega$  is fixed to the order of magnitude of mouse lungs ( $\approx 1 \text{ cm}^3$ ). Assuming that no mechanical interactions occur with the organ boundaries (for instance, the possible deformations of the organ due to the growth are neglected here), we supposed the domain  $\Omega$  large enough to consider the pressure on the boundaries as equal to the homeostatic pressure of the body. We model this by a Dirichlet boundary condition on the pressure:

$$\Pi = \Pi_{eq} \text{ on } \partial\Omega$$

Since  $\Pi$  is defined up to a constant, we can fix  $\Pi_{eq}$  equal to 0. Collecting (4) and (5), and considering the porosity  $k$  constant, we obtain  $\Pi$  to satisfy a Poisson equation with Dirichlet boundary conditions:

$$\begin{cases} -k\Delta\Pi = \gamma P \\ \Pi|_{\partial\Omega} = 0 \end{cases} \quad (6)$$

Similar models using more cellular species were used by Ribba, Colin and Schnell in [35] to predict efficacy of radiotherapy, and by Colin, Saut and colleagues in [11] to describe avascular tumour growth. In the latter, lack of nutrients and hypoxia were considered as essential limiting factors for growth and hence included in the model. In our study, we focused on a more phenomenological way to describe the fact that the tumour doubling time is increasing with the tumour size. A simple way to formalize this is to model the proliferation rate as a decreasing function of the pressure. This yields a simple model that captures the essential features of tumour expansion and is able to describe *in vivo* tumour growth.

### **Modelling the pressure-mediated inhibition of tumour growth**

Following the works of Montel et al. [36] and Stylianopoulos et al. [37,38], we considered that the growth rate of the tumour tissue decreases with the pressure exerted on the tissue. Therefore, we modelled the growth rate with a decreasing exponential law [36]:

$$\gamma(\Pi) = \gamma_0 \exp\left(\frac{-\Pi}{\Pi_0}\right) \quad (7)$$

where  $\Pi$  represents the pressure field,  $\gamma_0$  the maximal proliferation rate, and  $\Pi_0$  a characteristic pressure.

Under such a model, high pressure provokes decreased proliferation, but not apoptosis. Montel et al suggested that mechanical stresses have a poor effect on apoptosis, but also indicated that this could depend on the cell line and the experimental protocol [36].

**Model calibration:** To perform the study, we first wanted to fix the parameters of the model to realistic values to be able to infer reliable information from the simulations. We calibrated the model according to the growth of four metastases observed by MRI. These four tumours were selected because they were detectable during sufficient time points (n=4 for three of them, n=3 for one of them) and were manually segmented. Fig 5 shows the MR images, the numerical simulations starting from the initial shape with the parameters fitted on the volume, and the dynamics of the simulated volume for one of the mice. Spatial distributions of pressure ( $\Pi$ ) and proliferation rate ( $\gamma$ ) are presented in Fig S3. The three other fitted volume curves are presented in Fig S4. We observed that the model was able to describe the increase of the tumour volume for the four metastatic lesions. Table 2 presents the values of the two parameters for the four fitted growth curves.

### Fig 5. Spatial model fitting

(A): Coronal MRI data of the lungs at days 19 and 26. (B): The simulated growth by the model using the fitted parameters and starting from the real shape of the observed metastasis at day 19 on the coronal MRI slice. (C): Volume data are compared to simulations by the fitted model. The fit has been made on the volume only, considering the metastasis as spherical.

**Table 2: Values of the parameters resulting from the fit of each metastatic dynamics.**

	$\gamma_0$ (day <sup>-1</sup> )	$\Pi_0$ (Pa)
Meta 1	0.78	0.0026
Meta 2	1.01	0.00079
Meta 3	0.67	0.00067
Meta 4	0.8	0.00052

The value of  $\gamma_0$  corresponds to the maximal proliferation rate in optimal conditions of pressure. The values of  $\Pi_0$  are not reliable to real pressure values because they depend on the porosity, which is not a parameter, and because  $\Pi$  is computed up to a constant.

These fitted parameters provided a range to perform the tumour-tumour contact interactions study:

$$(\gamma_0, \Pi_0) \in (0.67, 1.01) \times (5.2 \cdot 10^{-4}, 2.6 \cdot 10^{-3}).$$

**Quantitative impact of pressure-mediated growth interactions:** We next aimed at studying the quantitative impact of the pressure that two neighbouring metastases exert on each other when they

grow, and the possibility of tumour merging. We focused more precisely on the two following issues:

- What is the quantitative impact of mechanical interactions between tumour foci?
- For a same initial metastatic burden, does the number of metastases have an impact on the dynamics (burden fractionation)?

*One tumour versus two tumours:*

Under classical non-spatial tumour growth laws (such as the Gompertz, power law, etc...), two independently growing tumours lead to a larger final burden than one single tumour having double initial size. However, these models do not provide any mechanistic explanation. Our spatial model reproduced this fact while additionally providing a possible mechanistic explanation (Fig 6A): in a larger tumour, there are more cells that proliferate, resulting in higher mechanical constraints than in a smaller one. The pressure is therefore higher in the larger tumour, resulting in faster saturation of tumour growth over time.

*Two interacting tumours versus two independent tumours:*

To quantify the impact of the mechanical interactions, we compared the two situations: (1) two metastases that grow independently (the final burden consists in summing-up the two burden) and (2) two metastases that are close to each other (the exerted pressure of one metastasis impacts the growth of the other).

The two configurations were studied and compared with 64 sets of parameters chosen in the parameter space established by the calibration. The results highlight the possibility for two metastases to mutually impair their growth by mechanical interactions. Indeed, by proliferating, the neighbouring tumours exert pressure on each other, which leads to a decrease in proliferation in comparison to distant growing tumour foci. More precisely, under the assumption of increasing doubling time with respect to the pressure, the calibrated model revealed substantial differences in tumour burden, as shown in Fig 6B. Among all the parameter sets, when two tumour foci interact, at the final time ( $T=7$  days, which corresponds to the time scale of the four metastatic growths) the loss of mass was  $31 \pm 1.5\%$  (mean  $\pm$  standard deviation) in comparison to distant growing tumour lesions. As an example, Fig 6C presents a simulation of two interacting tumours at four time points.

**Fig 6. Tumour-tumour spatial interactions**

(A) Three different configurations with a same initial burden: only one tumour, two close tumours, two far tumours. The dynamics in the three configurations are compared. (B) The final burden are compared in two configurations: two close tumours and two independent tumours. The mean burden on the 64 set of parameters are plotted with the standard deviations (difference of  $31\% \pm 1.5\%$  between the two distributions). (C) From left to right: time course of two interacting tumours growing and pushing each other. The parameters were fixed from one of the fitted MRI metastases. (D) The curve represents the evolution of the final burden with respect to the initial distance

between the two interacting tumours. The initial total burden and the parameters were taken to be the same as one of the four fitted metastases.

*Impact of the merging time:*

We observed in our data neighbouring metastases growing close to each other until merging (Fig 4). Mechanical interactions occurred at the time of merging, resulting in slower tumour growth. In terms of global dynamics, two different merging times generated two different dynamics. This merging time is equivalent to the initial distance between the two metastatic foci. We therefore studied the impact of the initial distance. Under our modelling assumptions, the interactions between two metastases decrease with the initial distance between them (Fig 6D). This means that the later the metastases merge, the larger the final burden is. When the initial distance between the tumours goes to 0, the burden corresponds to the burden of only one tumour. When the distance tends to infinite, the burden is equivalent to the burden of two independent tumours.

*Combined effects of mass fractionation and interactions between tumours:*

We studied the effect of the fractionation of a same burden for independent metastases and for interacting metastases with a distance of 0.2 mm between metastases. Fig S5 depicts the evolution of the burden as a function of the number of tumours in the case of independently growing tumours or tumours that mechanically interact. As shown, the difference between both situations increases with the number of metastases. For instance, for 18 metastases growing close to each other, the loss of mass from the independent case to the interactions case is 76.3% (to be compared to the 31% for two tumours).

**The merging hypothesis:** We did not, at first, consider any interactions between the metastatic foci and assumed the volume resulting from merging as equal to the sum of the metastatic foci volumes. We then performed four simulations with the four fitted parameter sets, starting from one cell, to estimate the required number of merging metastatic foci to obtain the respective (for the four fitted metastases) observed volumes at day 19 in seven days. Indeed we chose day 12 and not day 14 (first observed metastatic cells) as the starting day because the GFP signal started to rise at day 12 (Fig 2). The required numbers are presented in Table 3, with and without spatial interactions between the tumours.

We estimated the required number of metastatic foci to obtain the observed volumes in considering spatial interactions between merging foci. Each focus was assumed here to start from one cell and the foci were randomly distributed within the computational domain. To avoid metastatic foci too close from the domain boundaries and to allow the foci to merge together, the initial distance between the foci was constrained to 0.03 mm. Fig 7 depicts the simulations results. The number of required metastases reported in Table 3 has been estimated by dichotomy (the final burden increases with the number). Because the chosen initial distance between the foci was small, the mechanical interactions were maximal here. The estimated number is therefore probably

overestimated. Consequently, the two estimated numbers (with and without spatial interactions) give an approximate range for the exact required number.

**Fig 7. Simulation of metastatic foci merging**

From left to right: time course of merging metastatic germs. Each germ starts from one cell.

**Table 3: Number of required merging foci**

	Required number of metastases	
	Without spatial interactions	With spatial interactions
Meta 1	1337	2127
Meta 2	20	65
Meta 3	301	375
Meta 4	40	70

**There it is the number of required merging foci to obtain the metastatic sizes measured on the MR images for each followed metastasis.** Two cases are considered: with and without spatial interactions.

As can be seen in Table 3, the number of metastases was higher when interactions were taken into account. Because of potential variability, the estimated numbers of required metastatic foci may give only a rough estimate. With exception of one metastasis, the estimated numbers appear to be reasonable. For this tumour, the required number was between 1300 and 2100, which is probably too large to be biologically realistic.

Besides spatial interactions, another possible phenomenon involved could be the attraction and aggregation of circulating tumour cells. This hypothesis is discussed below.

## Discussion

Our study demonstrated that a naive theory of metastasis formation and growth, where the metastases grow independently from the remaining of the system, was not able to explain our experimental data with regard to sizes and number of metastatic lesions. To explain our findings, we proposed a simple hypothesis where merged metastatic foci are formed by passive motion. In order to quantitatively assess the validity of this theory, we derived a spatial model that was able to fit the growth of metastatic lesions in the lung. The model was also able to explain decay in the growth rate by a pressure-dependent mechanism.

Perhaps in contrast to a lot of efforts in cancer modelling, we combined various modelling techniques. We used ordinary differential equations for the description of tumour growth, structured population partial differential equations for metastatic colonies, nonlinear mixed-effects statistical tools for the estimation procedure and fluid dynamics-like partial differential equations for spatial tumour growth. We extended the results of [20] by showing that the model of [19] was also able to describe metastatic burden in a different animal model (kidney primary tumour in our case versus breast primary tumour in [20]) and a different quantification technique (GFP signal here, bioluminescence emission in [20]). Moreover, we compared the predictions of the model to imaging data obtained by MRI, which provided information on the number and size of the tumour lesions.

In our simulations, based on the rationale that lung capillaries have a diameter of the order of one tumour cell (20  $\mu\text{m}$ ) and that metastatic cells have lost expressions of cell-cell adhesion proteins such as cadherins [2], we assumed that metastases started from the size of one cell. This might be arguable and metastasis could start from tumour cell clumps [39]. To resolve this further and assess the robustness of our results, we performed the entire data analysis (fit of the total metastatic burden and resulting prediction of the metastatic size distribution) for values of the initial number of cells of 1, 10, 100 and 500 (Fig S6). While the hypotheses of  $V_0 = 1$  or 500 cells had still to be clearly rejected, an initial number of 100 cells could be in agreement with the data (although the largest metastasis at day 26 was still predicted much smaller in the model than in the data, with respective sizes of 3.58 and 13.6  $\text{mm}^3$ ). However, in animal experiments the vast majority of detaching tumour cell clumps has been shown to comprise less than 10 cells [39]. This suggests that, if the metastases started from a substantial amount of cells, the grouping of these cells probably occurred at the distant site, after extravasation from the blood circulation.

The standard thinking of metastatic initiation considers that metastatic foci, once established in a distant location, grow independently from each other (and from the primary tumour) [1,2,10,24–26]. No “merging hypothesis” has yet been reported in the literature. Our results suggest that spatial interactions have a substantial impact on the growth of multiple tumour lesions and that merging of independent metastatic foci should be considered in any future attempt to build a quantitative theory for the dynamics of metastasis formation.

The spatial model for tumour growth that we introduced is based on a pressure-induced decrease of the growth rate. Contact inhibition between cells is a mechanism for maintaining tissue homeostasis [3]. The ability of cancer cells to ignore these inhibition signals is a hallmark of cancer. In a recent study, Stylianopoulos et al showed that the uncontrolled proliferation of tumour cells results in mechanical stresses in the surrounding micro-environment of transplanted and human tumours [37]. Furthermore, they also showed that such an exerted pressure impairs *in vivo* proliferation via two mechanisms: reduced cancer cell proliferation in direct response to increased pressure, as well as a pressure-induced collapse of blood vessels within the tumour, leading to nutrient deficiency for tumour cells [38]. Based on these considerations, it seems relevant to consider that tumour expansion depends on the pressure. In our spatial growth model, the tissues motion is mediated by pressure gradients. It means that cells within a tumour tissue proliferate and that the exerted pressure pushes the neighbouring tissues. This pressure is not solely due to mechanical constraints (solid stresses, interstitial fluid pressure,...) exerted by the neighbouring cells on each other, but represents a more phenomenological pressure, that reflects the basic assumption of our modelling strategy for the tumour tissue being constituted by a fluid mixture in a porous medium.

Other studies of the spatial expansion of a tumour based on numerical simulations have also been reported. In [36], Montel et al discussed the fact that cells proliferate faster on the surface than in the bulk of a tumour spheroid. A classical reason is that nutrients do not penetrate deeply in the spheroid. However, Montel et al. suggested a mechanical effect due to the necessity for a cell to deform its environment in order to proliferate. In a *in silico* study on two-dimensional monolayers and three-dimensional spheroids, based on experimentally determined biophysical parameters, Drasdo and Höhme suggested that pressure conditions have a higher impact on doubling time than lack of nutrients [40]. Moreover, in [36], Montel et al. performed experiments where tumour cells were submitted to different pressure constraints and observed a decrease in proliferation when pressure was applied. In their study, simulation results that were compared to experimental ones showed an exponential decreasing of proliferation with pressure. However, the bulk and surface division rate were not affected equally by stresses. In our model, we used a similar pressure-mediated proliferation law traducing direct effects of mechanical stresses on proliferation as well indirect effects of proliferation on the micro environment (collapsing of blood vessels leading to lack of nutrients).

We used our spatial model to investigate whether the merging hypothesis could explain the unrealistically fast growth observed at initiation in the MRI. For one animal we obtained hardly plausible values (between 1300 and 2100 foci) which may indicate that besides merging by passive motion due to proliferation, other mechanisms such as chemokine-mediated cells attraction occur [5,41]. Circulating tumour cells may be attracted by some established niches and explain the abnormally fast volume expansions that we observed. Indeed, such chemokine-mediated attractions are presumed to play an important role for the pre-metastatic and metastatic niches establishment, in mediating myeloid and tumour cells attraction [5,41,42]. Moreover, chemo-attractants may play

a role in tissue tropism of metastatic cells [43]. Chemotactic gradients can attract metastatic cells that express the chemokine receptor to specific locations. We used this spatial model to investigate whether the merging hypothesis could explain the unrealistically fast growth observed at initiation in the MRI. For one animal we obtained hardly plausible values (between 1300 and 2100 foci) which may indicate that besides merging by passive motion due to proliferation, other mechanisms such as chemokines-mediated cells attraction occurs [5,41]. Circulating tumour cells may be attracted by some established niches and explain the abnormally fast volume expansions that we observed. Indeed, such chemokine-mediated attractions are presumed to play an important role for the pre-metastatic and metastatic niches establishment, in mediating myeloid and tumour cells attraction [5,41,42]. Moreover, chemo-attractants may play a role in tissue tropism of metastatic cells [43]. Chemotactic gradients can indeed attract metastatic cells that express the chemokine receptor to specific locations.

Our proposed hypotheses should be further experimentally reinforced, by, for example, implanting orthotopically and injecting intravenously two groups of cells into mice, each group being tagged with a different colour, and by quantifying single or mixed-coloured tumour foci. Furthermore, in vitro investigations by growing two (or more) tumour spheroids in close vicinity that would enter mechanical interactions and then quantifying the effect on global growth, would further reinforce our contentions.

Our methodology and results illustrate how a combined approach using multimodal biological data on one hand, and multimodal modelling analysis on the other, provides powerful insights into tumour biology and, in particular, into the metastatic process.

## Materials and methods

### Cell line and Mouse experiments

Ethical approval for all animal studies was obtained from the Institutional Animal Care and Use Committee of the INSERM Institute in accordance with the National Advisory Committee for Laboratory Animal Research Guidelines licensed by the French Authority. Animal facility: Animalerie mutualisée de Bordeaux 1, authorisation number: B33-522, Date: February 8<sup>th</sup>, 2012. Investigator: Andreas Bikfalvi (authorisation number: R-45GRETA-F1-10).

**RENCA-GFP cells:** The mouse renal adenocarcinoma cell line RENCA was cultured in RPMI media (Gibco) supplemented with 10% foetal calf serum, 1mM sodium pyruvate, 2mM glutamine, 100U/ml de penicillin and 100µg/ml streptomycin., at 37°C/5% CO<sub>2</sub>. RENCA-GFP cells were produced via infection of RENCA cells with a GFP lentivirus, a gift of Dr. C. Grosset (u889 Bordeaux).

**Orthotopic implantation of RENCA-GFP cells:** RENCA-GFP were cultured in exponential growth phase, and harvested by trypsinisation (Gibco). After washing in basal RPMI media, the cells were counted and concentration adjusted to 100000 cells per 25µl in basal media. 25µl of cell suspension was then injected underneath the renal capsule of the left kidney of female Balb/c mice aged 6 weeks.

**Tissue harvest:** Mice were sacrificed at the specified intervals and the left kidney (bearing the primary tumour) and lungs were dissected and snap frozen in liquid nitrogen. RNA was extracted using TRIzol Reagent (Life Technologies) as per the manufacturer's protocol.

**Reverse transcription and Q-RT-PCR:** RNA samples were quantified using a nanodrop ND-1000 spectrophotometer (Nanodrop Technologies). 1µg of total RNA was reverse transcribed to cDNA using High Capacity cDNA Reverse Transcription Kit (Applied Biosystems). Real-Time PCR was carried out using the Step One Plus Real-Time PCR system. Reactions were carried out in a total volume of 20µl containing 2ng of cDNA, Power SYBR Green PCR Mastermix (Applied Biosystems), and 200nM of each of the forward and reverse primers. The reaction conditions were as follows: 10 mins at 95°C followed by 40 cycles of 15 secs at 95°C and 1 min at 60°C.

Data were analysed using Step One Software v2.3. The housekeeping gene PPIA was used as an endogenous control to normalize for differences in the amount of total RNA in each sample. Expression of GFP is thus presented as an N-fold difference relative to the total RNA per sample.

The sequences of the primer used was as follows: eGFP: Forward primer 5'-CGACCACTACCAGCAGAACA-3' Reverse primer: 5'-GAACTCCAGCAGGACCATGT-3'

### MRI material and methods

**MRI material:** The experiments were carried out on a horizontal 7T magnet (Bruker Biospec 70/20, Germany), equipped with a 12 cm gradient insert capable of 660 mT/m maximum strength and 110 µs rise time. Lung imaging was performed using a quadrature emission/reception birdcage coil (inner diameter: 2.5 cm, 5 cm length).

Mice were anesthetized with 1.5% isoflurane in air during the imaging session. Mouse respiration was monitored during the entire experiment by using an air balloon placed on the abdomen (SA Instruments).

**MRI sequence:** A 3D water-selective balanced Steady State Free Precession sequence was used [44]. This sequence induces a T2-like contrast, allowing the detection of metastases with hyper-intense signals without injecting contrast agents [45]. The main parameters of the sequence were as follow: FOV=30×22×22; matrix=192×142×142; TE/TR=3.1/6.2ms; flip angle=20deg; reception bandwidth= 178kHz; number of excitation=1; acquisition time=2min3s. In order to suppress banding artifacts inherent to this sequence, the sum-of-square method was performed [46]. Thus, the total acquisition time was 8min12s.

## Numerical Methods

**Numerical methods to simulate the partial derivative equations model of spatial:** The system of partial derivative equations that models the spatial metastatic growth was solved with the following numerical methods:

- a Strang splitting method for the time scheme
- a fifth order Weno finite differences scheme for the spatial resolution
- A fixed point method to solve the non linear equation on the pressure

**Fitting method for the recovery of the PDE parameters:** The goal of the model calibration was not to precisely determine the best parameters for describing the growth of each metastatic lesion but to obtain a range of realistic parameters to perform the study. Moreover, segmentation measurement errors, which are probably important, were not estimated. For these reasons, we used a Monte Carlo method, which was easy to implement and parallelize. Boundaries of the parameter space have been first established by an analysis of the model and biological considerations for the parameters values.

Because we did not need a very high accuracy for the fits, we did not take the shape of the metastases into account. We considered them as spherical and fitted the model on the volume dynamics only.

## Acknowledgements

This study has been carried out within the frame of the LABEX TRAIL, ANR-10-LABX-0057 with financial support from the French State, managed by the French National Research Agency (ANR) in the frame of the « Investments for the future » Programme IdEx (ANR-10-IDEX-03-02).

Numerical experiments presented in this paper were carried out using the PlaFRIM experimental testbed, being developed under the Inria PlaFRIM development action with support

from LABRI and IMB and other entities: Conseil Régional d'Aquitaine, FeDER, Université de Bordeaux and CNRS (see <https://plafirm.bordeaux.inria.fr/>)

The authors would like to thank the PlanCancer from the National Cancer Institute (INCA) and the National Institute of Health and Medical Research (INSERM) for financial support of this project (MetaSys and MIMOSA grants).

## References

1. Talmadge JE, Fidler IJ. AACR centennial series: the biology of cancer metastasis: historical perspective. *Cancer Res.* 2010;70: 5649–5669.
2. Gupta GP, Massagué J. Cancer metastasis: building a framework. *Cell.* 2006;127: 679–695.
3. Hanahan D, Weinberg RA. Hallmarks of cancer: the next generation. *Cell.* 2011;144: 646–674.
4. O'Reilly MS, Holmgren L, Shing Y, Chen C, Rosenthal RA, Moses M, et al. Angiostatin: a novel angiogenesis inhibitor that mediates the suppression of metastases by a Lewis lung carcinoma. *Cell.* 1994;79: 315–328.
5. Kaplan RN, Riba RD, Zacharoulis S, Bramley AH, Vincent L, Costa C, et al. VEGFR1-positive haematopoietic bone marrow progenitors initiate the pre-metastatic niche. *Nature.* 2005;438: 820–827.
6. Kim M-Y, Oskarsson T, Acharyya S, Nguyen DX, Zhang XHF, Norton L, et al. Tumor self-seeding by circulating cancer cells. *Cell.* 2009;139: 1315–1326.
7. Ebos JML, Lee CR, Cruz-Munoz W, Bjarnason GA, Christensen JG, Kerbel RS. Accelerated metastasis after short-term treatment with a potent inhibitor of tumor angiogenesis. *Cancer Cell.* 2009;15: 232–239.
8. Chambers AF, Groom AC, MacDonald IC. Dissemination and growth of cancer cells in metastatic sites. *Nat Rev Cancer.* 2002;2: 563–572.
9. Chaffer CL, Weinberg R a. A perspective on cancer cell metastasis. *Science.* 2011;331: 1559–1564. doi:10.1126/science.1203543
10. Fidler IJ. The pathogenesis of cancer metastasis: the “seed and soil” hypothesis revisited. *Nat Rev Cancer.* 2003;3: 453–458.
11. Bresch D, Colin T, Grenier E, Ribba B, Saut O. Computational modeling of solid tumor growth: the avascular stage. *SIAM J Sci Comput.* 2010;32: 2321–2344.
12. Byrne HM. Dissecting cancer through mathematics: from the cell to the animal model. *Nat Rev Cancer.* 2010;10: 221–230.
13. Colin T, Iollo A, Lombardi D, Saut O. System identification in tumor growth modeling using semi-empirical eigenfunctions. *Math Model Methods Appl Sci.* 2012;22: 1250003–1250030.
14. Araujo RP, McElwain DLS. A history of the study of solid tumour growth: the contribution of mathematical modelling. *Bull Math Biol.* 2004;66: 1039–1091.
15. Benzekry S, Lamont C, Beheshti A, Tracz A, Ebos JML, Hlatky L, et al. Classical mathematical models for description and prediction of experimental tumor growth. *PLoS Comput Biol.* 2014;10: e1003800.
16. Liotta LA, Saidel GM, Kleinerman J. Stochastic model of metastases formation. *Biometrics.* 1976;32: 535–550.
17. Saidel GM, Liotta LA, Kleinerman J. System dynamics of metastatic process from an implanted tumor. *J Theor Biol.* 1976;56: 417–434.
18. Scott JG, Gerlee P, Basanta D, Fletcher AG. Mathematical modeling of the metastatic process BT - *Experimental Metastasis: Modeling and Analysis*. Experimental Metastasis: Modeling and Analysis. 2013.
19. Iwata K, Kawasaki K, Shigesada N. A Dynamical Model for the Growth and Size Distribution of Multiple Metastatic Tumors. *J Theor Biol.* 2000;203: 177–186.
20. Hartung N, Mollard S, Barbolosi D, Benabdallah A, Chapuisat G, Henry G, et al. Mathematical modeling of tumor growth and metastatic spreading: validation in tumor-bearing mice. *Cancer Res.* 2014;74: 6397–6407.

21. Benzekry S, Tracz A, Mastro M, Corbelli R, Barbolosi D, Ebos JML. Modeling spontaneous metastasis following surgery : An In vivo / in silico approach. Submitted. 2015;
22. Spratt JS, Meyer JS, Spratt JA. Rates of growth of human solid neoplasms: Part I. *J Surg Oncol.* 1995;60: 137–146.
23. Miyake H, Hara I, Gohji K. Relative Expression of Matrix Metalloproteinase-2 and Tissue Inhibitor of Metalloproteinase-2 in Mouse Renal Cell Carcinoma Cells Regulates Their Metastatic Potential Relative Expression of Matrix Metalloproteinase-2 and Tissue Inhibitor of Metalloproteinase-2. *Clin Cancer Res.* 1999; 2824–2829.
24. Talmadge JE, Fidler IJ. Evidence for the Clonal Origin of Spontaneous Metastases. *Science (80- ).* 1982;217: 361–363.
25. Fidler IJ, Talmadge JE. Evidence that intravenously derived murine pulmonary melanoma metastases can originate from the expansion of a single tumor cell. *Cancer Res.* 1986;46: 5167–5171.
26. Klein CA. Parallel progression of primary tumours and metastases. *Nat Rev Cancer.* 2009;9: 302–312.
27. Wheldon TE. *Mathematical models in cancer research.* 1988.
28. Casey AE. The Experimental Alteration of Malignancy with an Homologous Mammalian Tumor Material : I . Results with Intratesticular Inoculation. *Am J Cancer.* 1934;21: 760–775.
29. Laird AK. Dynamics of tumor growth. *Br J Cancer.* 1964;18: 490–502.
30. Norton L. A Gompertzian model of human breast cancer growth. *Cancer Res.* 1988;48: 7067–7071.
31. Lavielle M. *Mixed Effects Models for the Population Approach. Models, Tasks, Methods and Tools.* 2014.
32. Mathworks T. *Matlab with statistics and optimization toolboxes.* Natick, Massachusetts, United States; 2013.
33. Hartung N. Efficient resolution of metastatic tumor growth models by reformulation into integral equations. *Discret Contin Dyn Syst Ser B A J Bridg Math Sci.* 2015;20: 445–467.
34. Ambrosi D, Preziosi L, Modica M. On the closure of mass balance models for tumor growth. *Math Model Method A Appl Sci.* 2002;12: 737–754.
35. Ribba B, Colin T, Schnell S. A multiscale mathematical model of cancer, and its use in analyzing irradiation therapies. *Theor Biol Med Model.* 2006;3: 7.
36. Montel F, Delarue M, Elgeti J, Vignjevic D, Cappello G, Prost J. Isotropic stress reduces cell proliferation in tumor spheroids. *New J Phys.* 2012;14: 55008.
37. Stylianopoulos T, Martin JD, Chauhan VP, Jain SR, Diop-Frimpong B, Bardeesy N, et al. Causes, consequences, and remedies for growth-induced solid stress in murine and human tumors. *Proc Natl Acad Sci.* 2012;109: 15101–15108. doi:10.1073/pnas.1213353109
38. Stylianopoulos T, Martin JD, Snuderl M, Mpekris F, Jain SR, Jain RK. Coevolution of solid stress and interstitial fluid pressure in tumors during progression: implications for vascular collapse. *Cancer Res.* 2013;73: 3833–3841.
39. Liotta LA, Kleinerman J, Saidel GM. The Significance of Hematogenous Tumor Cell Clumps in the Metastatic Process. *Cancer Res.* 1975; 889–894.
40. Drasdo D, Höhme S. A single-cell-based model of tumor growth in vitro: monolayers and spheroids. *Phys Biol.* 2005;2: 133–147.
41. Hiratsuka S, Watanabe A, Aburatani H, Maru Y. Tumour-mediated upregulation of chemoattractants and recruitment of myeloid cells predetermines lung metastasis. *Nat Cell Biol.* 2006;8: 1369–1375. doi:10.1038/ncb1507

42. Psaila B, Lyden D. The metastatic niche: adapting the foreign soil. *Nat Rev Cancer*. 2009;9: 285–293. doi:10.1038/nrc2621
43. Joyce J a, Pollard JW. Microenvironmental regulation of metastasis. *Nat Rev Cancer*. 2009;9: 239–252. doi:10.1038/nrc2618
44. Ribot EJ, Wecker D, Trotier A, Lefrançois W, Thiaudière E, Franconi, JM and MS. Water selective imaging and bSSFP banding artifact correction in humans and small animals at 3T and 7T, respectively. *J Magn Reson Imaging Under Revis*.
45. Ribot EJ, Martinez-Santesteban FM, Simeanea C, Steeg PS, Chambers AF, Rutt BK, et al. In vivo single scan detection of both iron-labeled cells and breast cancer metastases in the mouse brain using balanced steady-state free precession imaging at 1.5 T. *J Magn Reson Imaging*. 2011;34: 231–238. doi:10.1002/jmri.22593
46. Miraux S, Massot P, Ribot EJ, Franconi JM, Thiaudiere E. 3D TrueFISP imaging of mouse brain at 4.7T and 9.4T. *J Magn Reson Imaging*. 2008;28: 497–503. doi:10.1002/jmri.21449

## Supporting Information

### **S1 Fig. Population fit of the primary tumour dynamics**

The initial volume is calibrated during the fit. Right panel: the points represent the data, the curve represents the median dynamics, and the dashed curves the percentiles. Left panel: values of the parameters resulting from the population fit of the primary tumour dynamics. NSE: normalized standard error.

### **S2 Fig. 1 vs 2 tumours**

At the top: Two tumours growing under an exponential law give rise to the same final total volume than one tumour with the same initial total volume; At the bottom: Two tumours growing under a Gompertz law give rise to a bigger final volume than one tumour with the same initial total volume

### **S3 Fig. Spatial simulation of a lung metastasis**

The simulated growth by the model using the fitted parameters and starting from the real shape of the observed metastasis at day 19 on the coronal MRI slice. Time course of the tumour density (up), pressure (middle), and proliferation rate fields. From left to right: day 0, day 3 and day 7.

### **S4 Fig. Four individual metastatic growths fitted with the spatial model**

### **S5 Fig. Evolution of the final burden with respect to the number of interacting metastases**

Results of the simulation (Day 7) with different numbers of metastases: 4, 12 and 22. The parameters values are chosen among the sets of fitted parameters on individual metastatic growths.

### **S6 Fig. Time course of the macro-metastases size distribution for different initial metastatic cells aggregates**

Top to down: Simulation of the mathematical formalism of the naive theory (i.e. dissemination and independent growth of the resulting tumor foci), using the parameter values inferred from the total metastatic burden data (total GFP signal in the lungs) using four different initial numbers of initiating metastatic cells. The results are compared to observations of macro-metastases numbers and sizes in one mouse on MRI data.

### **S1 File. Simulation of a lung metastasis starting from the shape of the segmented metastatic focus**

The parameters have been calibrated on the volume dynamics of the metastasis

### **S2 File. Simulation of two neighboring tumours that are growing and pushing each other by passive motion**

### **S3 File. Simulation of merging metastatic foci**

# A modeling study of metastatic initiation and tumor-tumor spatial interactions: Figures

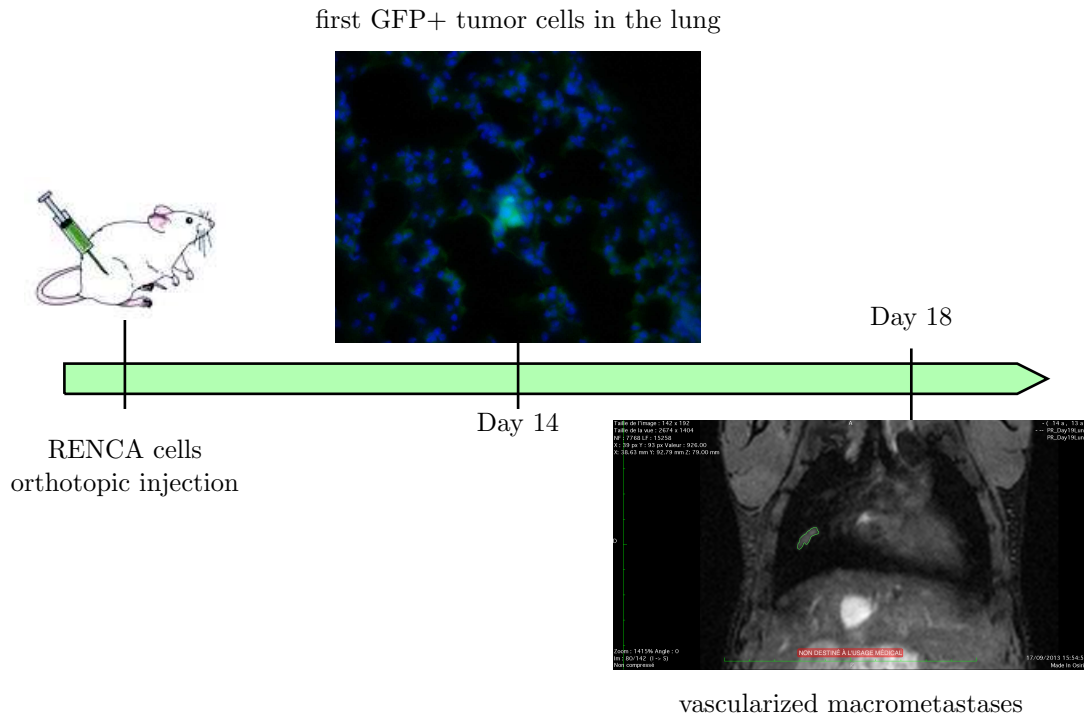


Figure 1: At day 14 after GFP+ RENCA cells injection, the first tumor cells are observed in the lungs; At day 18, first macrometastases are observed at MRI

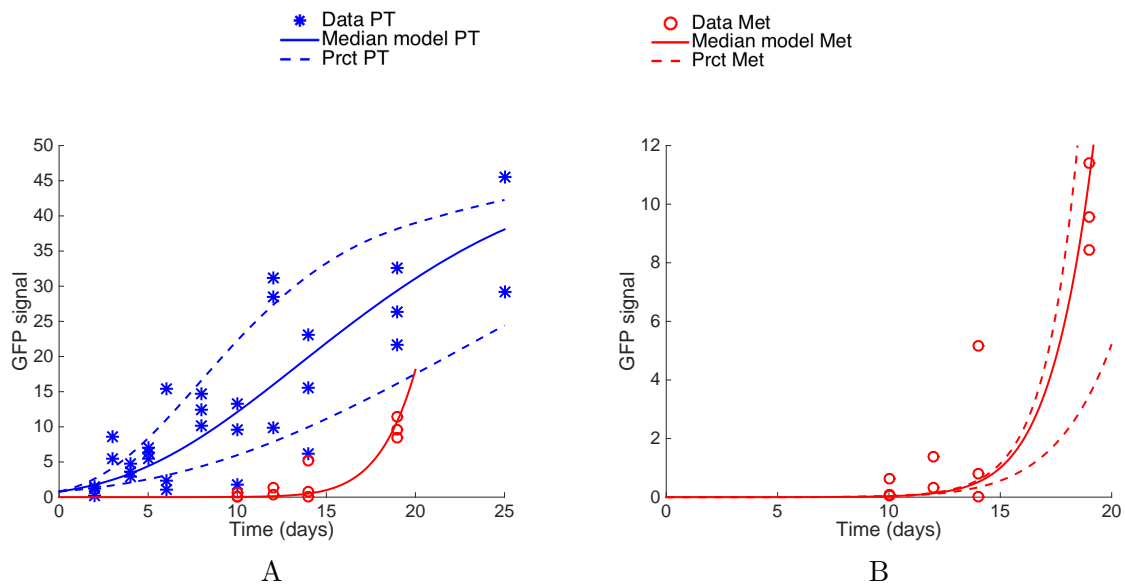
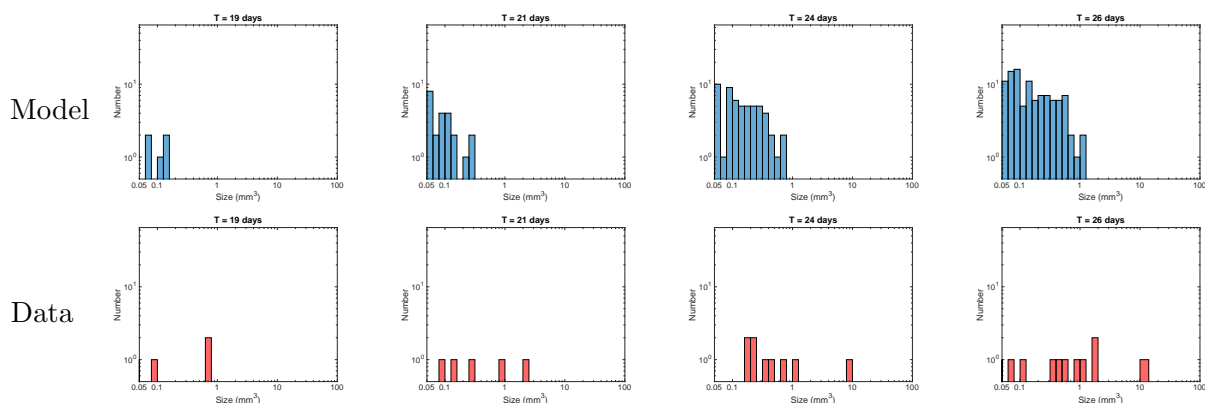


Figure 2: A: Fits of the primary tumor and metastatic burden dynamics, under a mathematical model assuming independent growth of each secondary tumor and using mixed-effects for statistical representation of the population distribution of the parameters and measurement error. B: Fit on the metastatic burden. PT= Primary Tumor. Met = Metastatic burden. Prct = percentile



T	19		21		24		26	
	Data	Model	Data	Model	Data	Model	Data	Model
Number	4	5	5	23	9	55	11	102
Macro-burden ( $\text{mm}^3$ )	1.58	0.52	3.55	2.54	11.51	10.4	21.16	23.4
Size of largest met ( $\text{mm}^3$ )	0.78	0.146	2.19	0.301	8.17	0.693	13.6	1.06

Figure 3: Time course of the macro-metastases size distribution: naive model versus observations. Top row: Simulation of the mathematical formalism of the naive theory (i.e. dissemination and independent growth of the resulting tumor foci), using the parameter values inferred from the total metastatic burden data (total GFP signal in the lungs). Only tumors larger than the visible threshold at MRI ( $0.05 \text{ mm}^3$ ) were plotted. Bottom row: Observations of macro-metastases numbers and sizes in one mouse on MRI data.

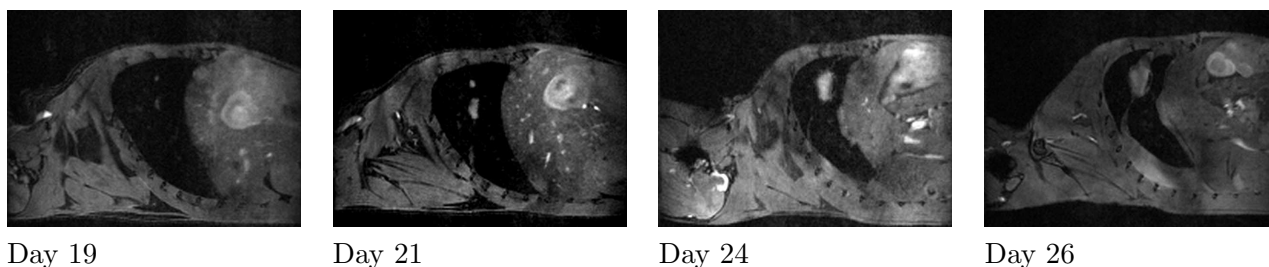


Figure 4: From left to right: Sagittal slide of the lungs from Day 19 to Day 26 of the same mouse: Two tumors are growing close to each other and they merge between Day 21 and 24

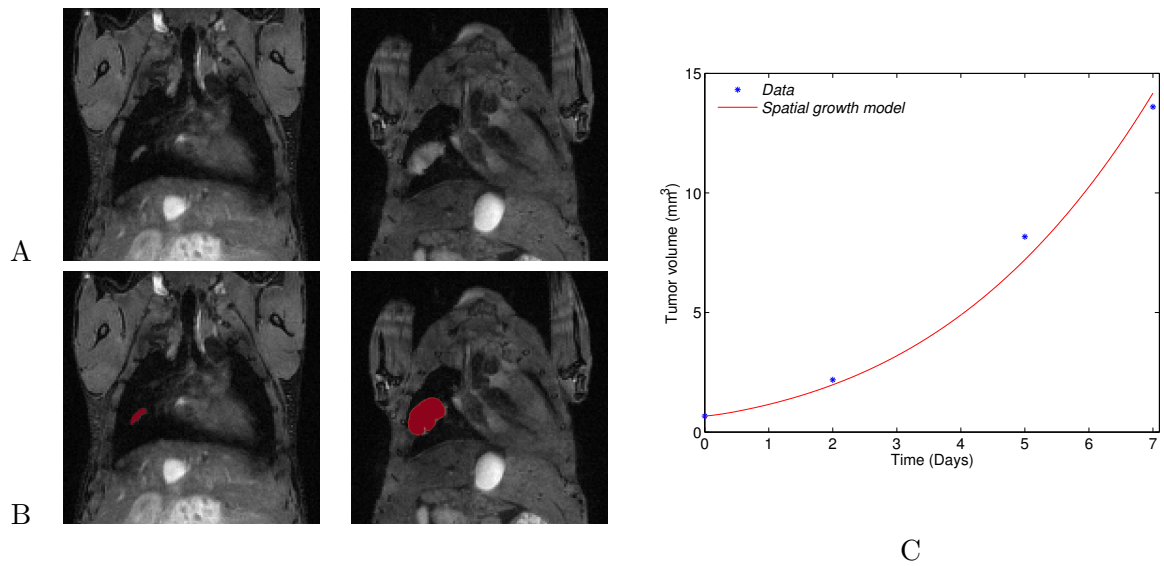


Figure 5: A: Coronal MRI data of the lungs at days 19 and 26. B: the simulated growth by the model using the fitted parameters and starting from the real shape of the observed metastasis at day 19 on the coronal MRI slice. C: volume data are compared to simulations by the fitted model. The fit has been made on the volume only, considering the metastasis as spherical.

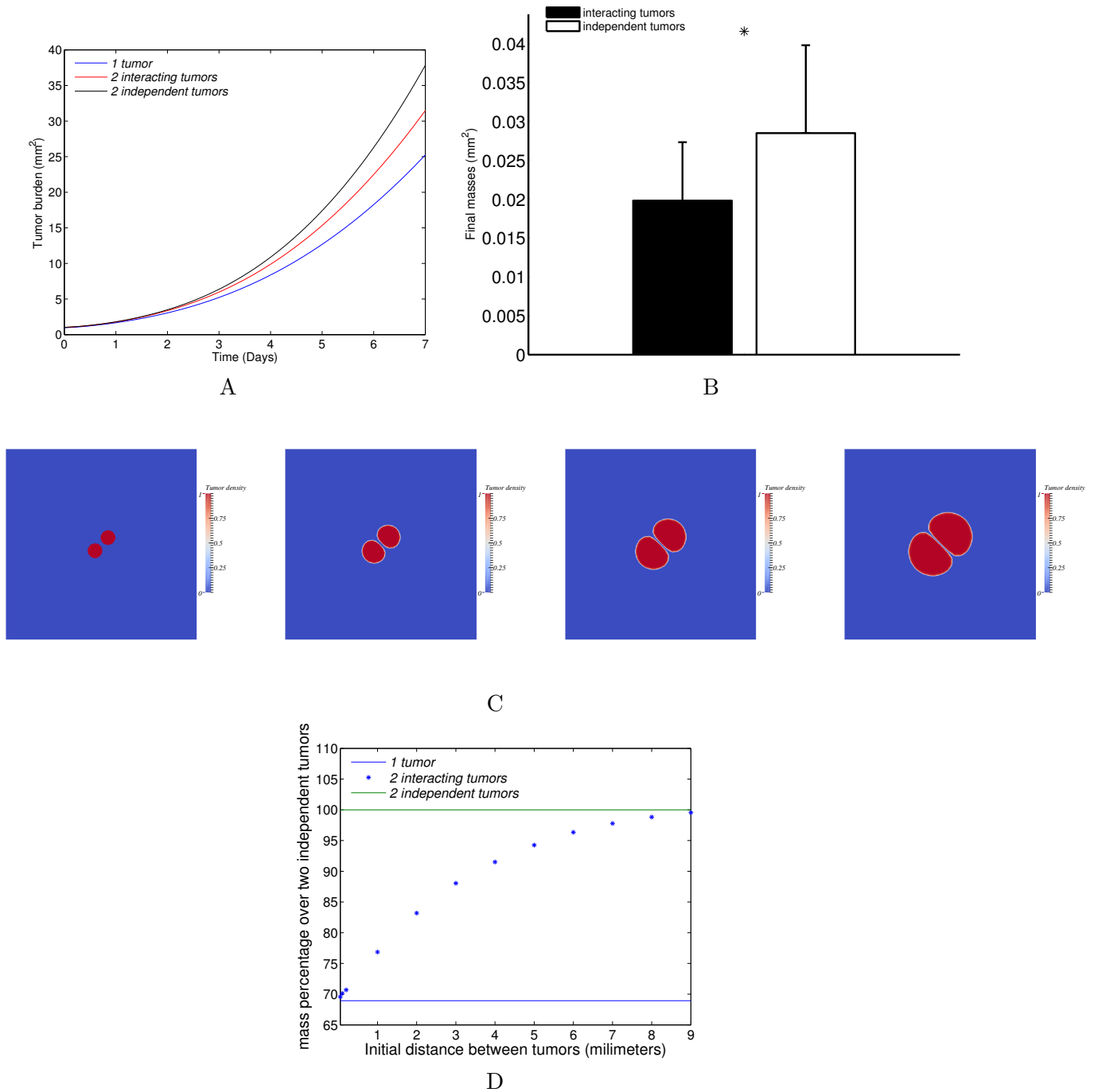


Figure 6: A: Three different configurations with a same initial burden: only one tumor, two close tumors, two far tumors. The dynamics in the three configurations are compared. B: The final burden are compared in two configurations: two close tumors and two independent tumors. The mean burden on the 64 set of parameters are plotted with the standard deviations (difference of  $31\% \pm 1.5\%$  between the two distributions). C: from left to right: dynamics of two interacting tumors growing and pushing each other. The parameters were fixed from one of the fitted MRI metastases. D: the curve represents the evolution of the final burden with respect to the initial distance between the two interacting tumors. In the simulations and results presented here, the initial total burden was taken to be the same as one of the four fitted metastases

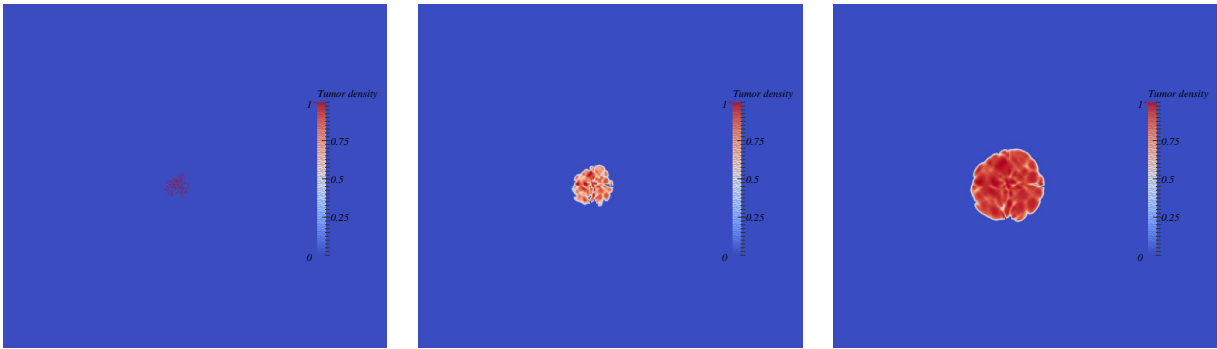
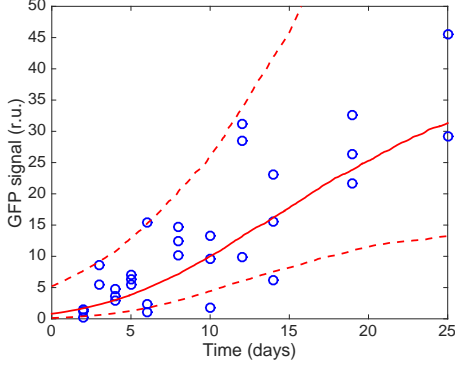


Figure 7: From left to right: the time course of merging metastatic germs. Each germ starts from one cell.

# A modeling study of metastatic initiation and tumor-tumor spatial interactions: Supplementary Figures



Par.	Unit	Median value	NSE (%)
$\alpha$	$[day^{-1}]$	0.384(20.07)	25.4
$\beta$	$[day^{-1}]$	0.1(14.36)	39.1
$V_0$	$[GFP(r.u.)]$	0.796(695.8)	81.6

Figure 1: Population fit of the primary tumor dynamics. The initial volume is calibrated during the fit. At right: the points represent the data, the curve represent the median dynamics, and the dashed curves the percentiles. At left: values of the parameters resulting from the population fit of the primary tumor dynamics. NSE: normalized standard error.

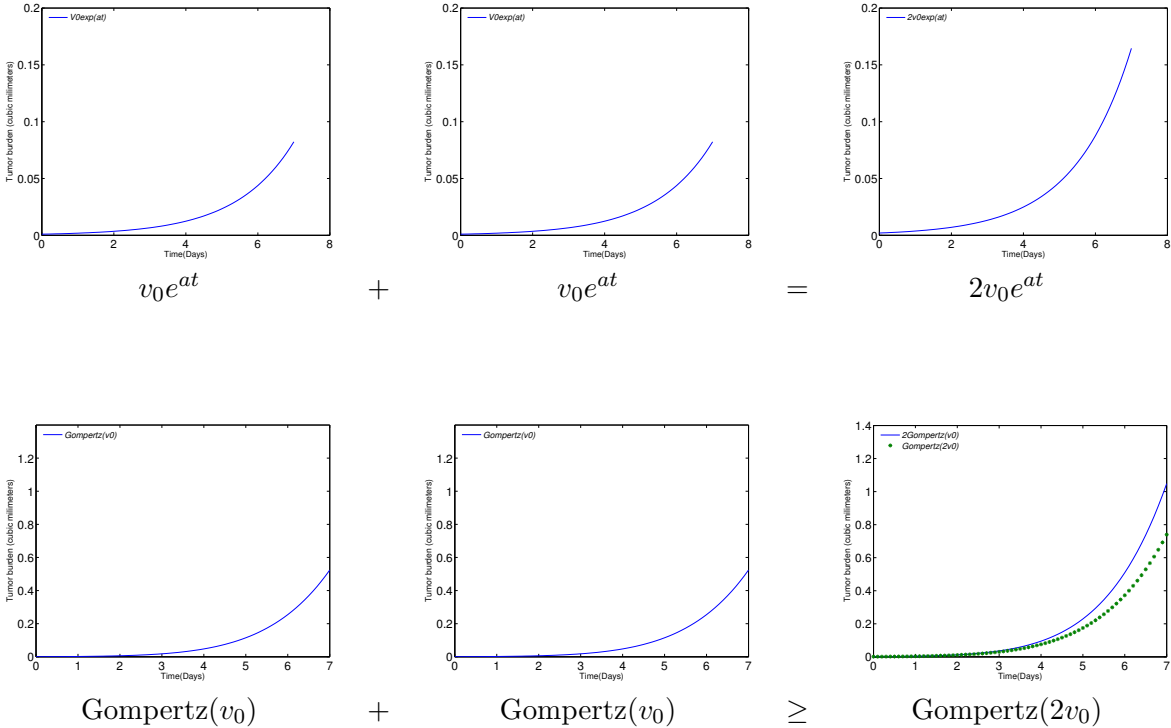


Figure 2: At the top: Two tumors growing under an exponential law give rise to the same final total volume than one tumor with the same initial total volume; A the bottom: Two tumors growing under a gompertz law give rise to a bigger final volume than one tumor with the same initial total volume

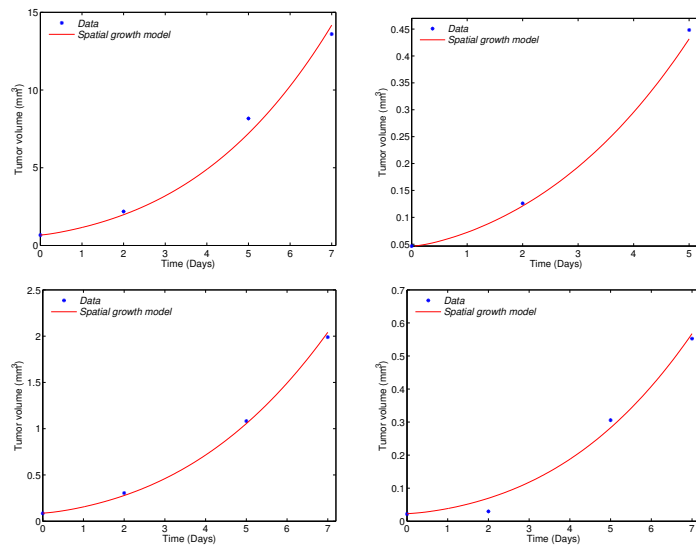


Figure 3: Four individual metastatic growths fitted with the spatial model.

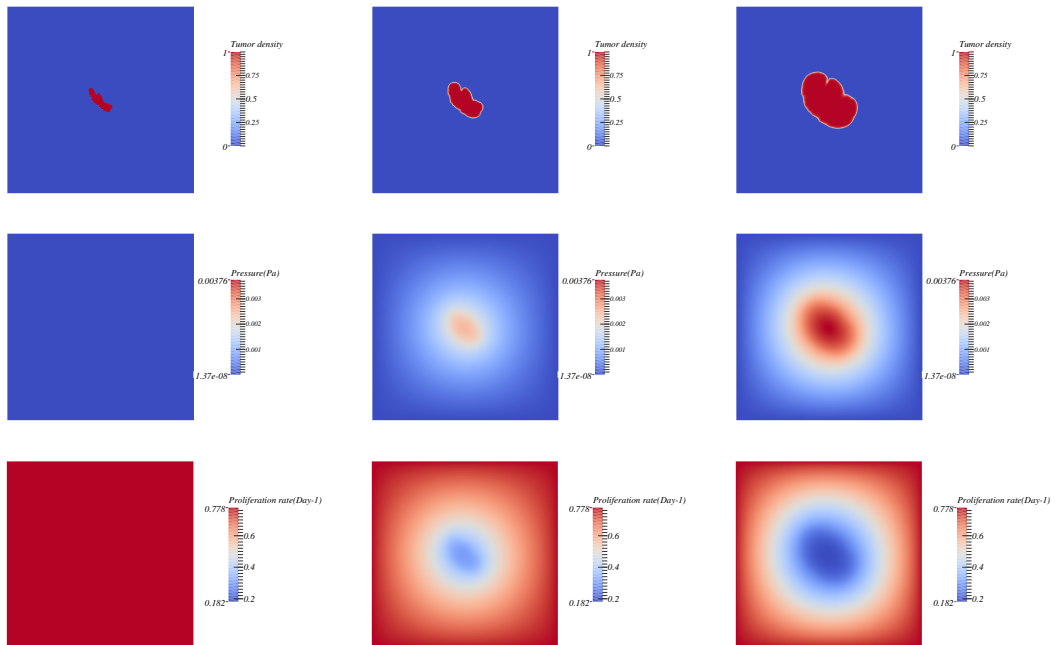


Figure 4: The simulated growth by the model using the fitted parameters and starting from the real shape of the observed metastasis at day 19 on the coronal MRI slice. Time course of the tumor density (up), pressure (middle), and proliferation rate fields. From left to right: day 0, day 3 and day 7

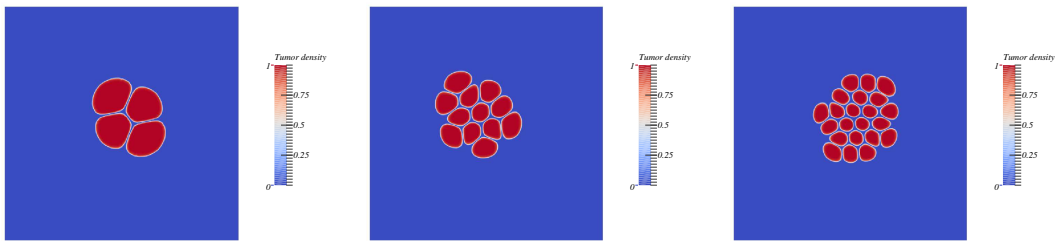
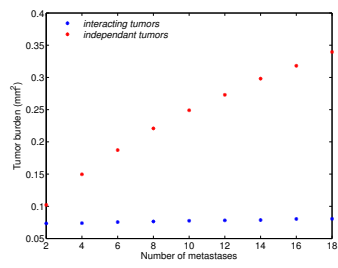


Figure 5: Top: Evolution of the final burden with respect to the number of interacting metastases. Bottom: results of the simulation (Day 7) with different numbers of metastases: 4, 12 and 22